Experimental Observation of Multistability and Dynamic Attractors in Silicon Central Pattern Generators

Le Zhao* and Alain Nogaret†
Department of Physics, University of Bath, Bath BA2 7AY, UK

We report on the multistability of chaotic networks of silicon neurons and demonstrate how spatiotemporal sequences of voltage oscillations are selected with timed current stimuli. A 3 neuron central pattern generator was built by interconnecting Hodgkin-Huxley neurons with mutually inhibitory links mimicking gap junctions. By systematically varying the timing of current stimuli applied to individual neurons, we generate the phase lag maps of neuronal oscillators and study their dependence on the network connectivity. We identify up to 6 attractors consisting of triphasic sequences of unevenly spaced pulses propagating clockwise and anti-clockwise. While confirming theoretical predictions, our experiments reveal more complex oscillatory patterns shaped by the ratio of the pulse width to the oscillation period. Our work contributes to validating the command neuron hypothesis.

PACS numbers: 02.30.Zz,05.45.Tp,87.19.L-

I. INTRODUCTION

Central pattern generators (CPGs) are small neural networks that provide the rhythms and coordination sequences which are essential for life. CPGs control heart rate [1, 2], respiration [2, 3], digestion [4, 5], circadian rhythm [6], locomotion [7, 8], escape mechanisms [9], coughing and sneezing [10]. A key challenge for nonlinear science is to understand how networks of competing neurons adapt to physiological feedback [11] to produce useful rhythmic patterns. One way in which this can be done is through changes in network connectivity. Experiments on the stomatogastric ganglion of the lobster [12, 13] have shown that the frequency of network oscillations is finely tuned by neuromodulatory substances which control synaptic delays. The release of "cocktails" of neurotransmitters can modify the network connectivity to a degree where new rhythms are induced [14]. Adaptation through network reconfiguration has been modelled in hardware by Nakada et al. [15] who succeeded in reproducing different gaits using a modular network architecture. It has separately been suggested that CPGs may use the multistability of coupled nonlinear oscillators [16] to produce different rhythmic patterns [17, 18]. Within this picture, stable spatiotemporal sequences evolve from initial conditions imparted by the timing of current stimuli. An experimental proof of stimulus induced switching would substantiate the hypothesis that Nature has evolved the ability to use currents input by sensory receptors and command neurons to generate different rhythmic sequences [17, 18]. The direct observation of stimulus induced switching in biological experiments is complicated by the large number of variables and unknown parameters which often require a statistical treatment. Numerical simulations in contrast have successfully mapped switching and multistability in inhibitory networks but these have been restricted to networks of small size [16, 19, 20]. Canavier et al [16] reduced the multivariate problem of the three neuron network to a two-dimensional problem allowing phase portraits to be mapped as a function of the dephasing between two neurons and the third neuron. Three stable attractors were identified as clockwise and anticlockwise firing sequences, supplemented by a third state where all three neurons fire in phase. Wojcik et al [19, 20] have examined the dependence of the phase maps on network connectivity and predicted the formation of up to 5 attractors including clockwise and anticlockwise sequences, and three further modes having two neurons firing in phase with each other but out of phase with the third. Electrically induced switching by networks of competing neurons is a plausible mechanism for explaining the reflex locomotor response observed in escape mechanisms [9] and in the switching between different gaits [21, 22]. These rhythmic patterns are robust against perturbations and noise as they rely on the propagation of neuronal activity along stable heteroclinic orbits surrounded by large basins of attraction.

Here we report on the realization of a chaotic network of silicon neurons and the experimental study of its oscillations. Multiple attractors form which are associated with stable firing sequences. By applying timed current stimuli to individual neurons, we are able to switch the state of the network. Our CPG consists of three neurons, modelling the Na, K and leakage channels [23]. These neurons compete through reciprocally inhibitory links. By systematically varying the time delay between current steps, we map the phase response trajectories emanating from every point in phase space. The transient state is found to evolve towards dynamic limit cycles consisting of triphasic sequences carrying clockwise or anticlockwise momentum. State degeneracy is further lifted by the non isochronous firing of neurons within the cy-

* Present address: Institute of Biomedical Engineering, School of Control Science and Engineering, Shandong University, Shandong 250061, P.R.China
† Corresponding author: A.R.Nogaret@bath.ac.uk

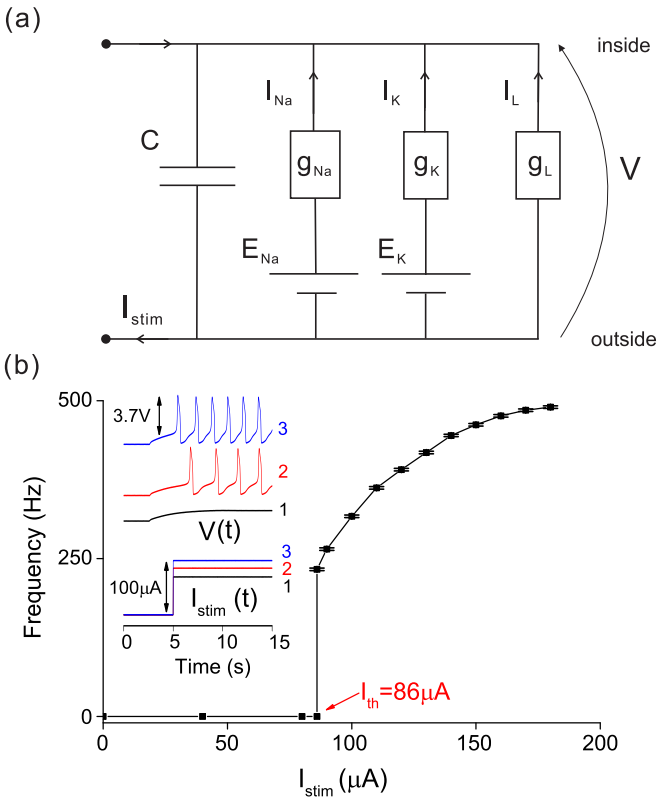

FIG. 1. (color online) (a) Electrical circuit of the silicon neuron. C is the membrane capacitance; g_{Na}, g_K, and g_L are the Na, K and leakage conductances; E_{Na} and E_K are the reversal potentials. The injection of a depolarizing current, I_{stim}, induces oscillations of the membrane voltage V. (b) Membrane voltage oscillations evoked by current stimulation of amplitude 60μA (black curve, labelled 1), 80μA (red curve, 2), 100μA (blue curve, 3). Main panel: excitatory response with current threshold: $I_{th} = 86\mu$A.

cle. We find that rhythmic sequences self-organize into stable patterns of two consecutive pulses firing out of phase with the third. As a result, rhythms are shaped by the ratio of the pulse width to the oscillation period. We study the stability of the different attractors as a function of the network connectivity and the amplitude of input currents. The clockwise basin of attraction is found to expand when anticlockwise projecting inhibition increases relative to clockwise inhibition and vice versa.

Our work shows that analog networks provide an alternative to numerical simulations for investigating the properties of winnerless competition networks [24, 25]. In particular, the properties of larger networks which are difficult to simulate numerically [26] are more easily accessible in experimental networks which compute in real time according to the laws of Physics. Our findings pave the way to devices that make constructive use of chaotic dynamics to achieve intelligent neurostimulation [27, 28] and motor coordination.

Following this introduction (section I), we report on the methodology (section II) and on the results (section III) before discussing the significance of the results in relation to existing theories (section V).

II. EXPERIMENTAL

Our silicon neuron models the electrical equivalent circuit of the neuron membrane (Fig.1(a)). Kirchoff current and voltage laws allow to write the dependence of the membrane voltage V on the stimulation current I_{stim} as:

$$C\frac{dV}{dt} = g_{Na}(E_{Na}-V)+g_K(E_K-V)+g_LV+I_{stim} \quad (1)$$

where C is the membrane capacitance, E_{Na} and E_K are the reversal potentials of sodium and potassium ions. The leakage reversal potential [29] is omitted as here it only adds a correction to the membrane resting potential from chloride and other ion species and has no effect on dynamical properties. The circuits emulating the sodium and potassium conductances, $g_{Na}(V,t)$ and $g_K(V,t)$, are described by Mahowald and Douglas [23]. These circuits model the gate variables m,h and n of the Hodgkin-Huxley model [29] with three gate currents I_m, I_h and I_n which control the conductances of two Metal Oxide Field Effect Transistors representing $g_{Na}(I_m, I_h)$ and $g_K(I_n)$. The sodium activation gate opens with probability m when V increases above threshold voltage V_m. The inactivation gate closes with probability $1-h$ when V increases above threshold voltage V_h. The potassium activation gate opens with probability n when V increases above threshold V_n. The activation and inactivation curves are modelled by differential transistor pairs which give the sigmoid voltage dependence:

$$I_x(V_{\tau x}) = \overline{I}_x\frac{1}{2}\left[1+\tanh\left(\frac{V_{\tau x}-V_x}{dV_x}\right)\right]. \quad x\equiv\{m,h,n\} \quad (2)$$

The maximum current $\overline{I}_x$ passing through the differential pair sets the maximum value of the ionic conductances $\overline{g}_{Na}$ and $\overline{g}_K$ in the Hodgkin-Huxley model. The experimenter controls this current with the gate voltage of a current source transistor. The $V_{\tau x}$ variable is effectively a time delayed membrane voltage which, within Eq.2, accounts for the delayed opening of gate x. This delay is implemented in VLSI by a low pass filter which integrates the membrane voltage according to:

$$\frac{dV_{\tau x}}{dt} = \frac{V-V_{\tau x}}{\tau_x}. \quad (3)$$

This equation is equivalent to:

$$\frac{dx(V,t)}{dt} = \frac{x_\infty(V)-x(V,t)}{\tau_x}, \quad x\equiv\{m,h,n\} \quad (4)$$

in the Hodgkin-Huxley model. τ_m, τ_h and τ_n are the gate time delays; $m_\infty(V)$, $h_\infty(V)$ and $n_\infty(V)$ are the gate

TABLE I. Analogue neuron parameters

Parameter	Description	Value
C	Membrane capacitance	10nF
$\overline{g}_{Na}$	Max. Na conductance	0.40mS
$\overline{g}_K$	Max. K conductance	0.32mS
g_L	Leak conductance	0.10mS
E_{Na}	Na potential	5V
E_K	K potential	0V
τ_m	Na activation delay	0ms
τ_h	Na inactivation delay	0.02ms
τ_n	K activation delay	0.10ms
V_m	Na activation threshold	1.52V
V_h	Na inactivation threshold	4.76V
V_n	K activation threshold	1.26V
dV_m	Na activation width	+0.6V
dV_h	Na inactivation width	-0.6V
dV_n	K activation width	+0.6V

variables in the steady state. Neuron gate thresholds V_x, time delays τ_x and maximum ion conductances are thus controlled with the gate voltages of MOSFETs.
We set these parameters to the values listed in Table I. The width of the gate opening region dV_x has a fixed value determined by the structural parameters of our field effect transistors (ALD1106 and ALD1107), namely the gate width, gate length, and gate oxide capacitance per unit area. dV_x is positive for ionic activation gates and negative for inactivation gates (Table I).

A depolarizing current I_{stim} is injected through the neuron circuit to probe its excitatory response - see Fig.1(b). Current stimulation shifts the membrane resting potential $\frac{g_{Na}E_{Na}+g_KE_K}{g_{Na}+g_K+g_L}$ by $\frac{I_{stim}}{g_{Na}+g_K+g_L}$ which in turn causes the voltage gated conductances $g_{Na}(V)$ and $g_K(V)$ to increase. The sodium gate opens first which drives V towards E_{Na} as $g_{Na} \gg g_K, g_L$. When the sodium inactivation gate closes and the potassium gate begins to open, $g_K \gg g_{Na}, g_L$ and V tends towards E_K. Under constant current stimulation, the membrane voltage oscillates between E_{Na} and E_K. We measure the onset of these oscillations by stimulating the neuron with currents of increasing magnitude. The oscillation threshold is $I_{th} = 86\mu$A. The frequency of neuron oscillations increases when current stimulation increases above the threshold (Fig.1(b)).

Neurons are interconnected with the VLSI differential transconductance amplifiers shown in Fig.2(a) which inject a post-synaptic current proportional to the voltage difference between the pre- and post-synaptic neurons. The interconnect in Fig.2(a) is inhibitory as it injects a hyperpolarizing post-synaptic current when the pre-synaptic neuron depolarizes. This is shown in the I-V curves of Fig.2(b) which have a linear central region given by: $I_{post} = g(V_{max})(V_{post} - V_{pre})$ [30]. This coupling may be likened to a gap junction [31]. We were able to tune its conductance $g(V_{max})$ in the range 0 to 900μS with V_{max} (Fig.2(c)). Our inhibitory links are used in all networks studied below. However for

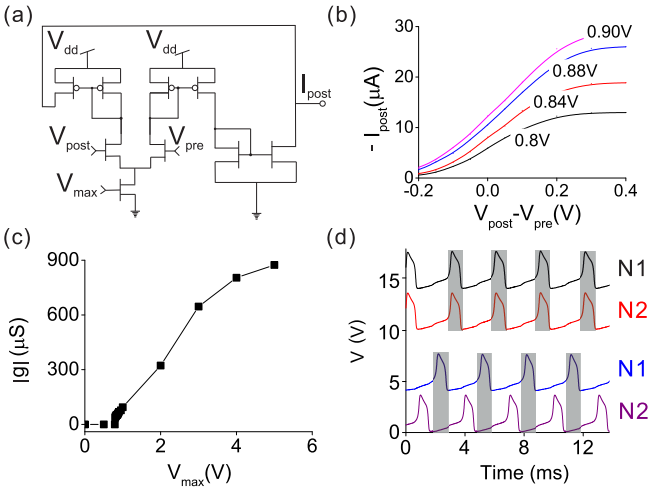

FIG. 2. (color online) (a) Inhibitory link injecting a hyperpolarizing current $I_{post} = g(V_{max})(V_{post} - V_{pre})$ in the post-synaptic neuron. (b) Experimental dependence of the post-synaptic current on $V_{post} - V_{pre}$ at different values of V_{max}. (c) Dependence of the link conductance on V_{max}. (d) Oscillations of a neuron pair coupled via reciprocally excitatory (top) and reciprocally inhibitory links (bottom). $I_{stim} = 100\mu$A, $g_{12} = 23.5\mu$S, $g_{21} = 37.2\mu$S.

the sake of completeness, we also verified that swapping V_{pre} and V_{post} in Fig.2(a) gives excitatory action through $I_{post} = g(V_{max})(V_{pre} - V_{post})$. Fig.2(d) compares the oscillations of two neurons coupled via mutually excitatory links (top) and mutually inhibitory links (bottom). Neuron oscillations are found to synchronize in-phase when coupling is excitatory and out-of-phase when it is inhibitory confirming the mechanism of action of our interconnects [32]. We used conductances $g_{12} = 23.5\mu$S and $g_{21} = 37.2\mu$S.

We then built the CPG of Fig.3 by interconnecting 3 neurons with pairs of reciprocally inhibitory links g_{ij}, $i, j = 1, 2, 3$. In addition to post-synaptic currents, neurons receive external stimulation from timed current steps whose time delays Δt_{12} and Δt_{13} set the initial conditions for network oscillations. Current stimulation was applied by a data acquisition card (NI PCI6259) controlled by a computer. The current amplitude was set just above the threshold at I_{stim} =100μA to induce low frequency voltage oscillations. This was important to maximize the number of phase lag data points that could be acquired during the time interval of transient oscillations. The computer systematically varied Δt_{12} and Δt_{13} between 0 and the period of oscillations T in steps of $0.05T$. After each current delay was applied, the computer recorded the transient oscillations of individual neurons over approximately 50 periods. In this way we probed the network dynamics for all initial conditions.

The network connectivity was chosen to induce chaotic dynamics which was necessary to allow attractors to form. This required reciprocally inhibitory links to have asymmetric conductances as otherwise neurons oscilla-

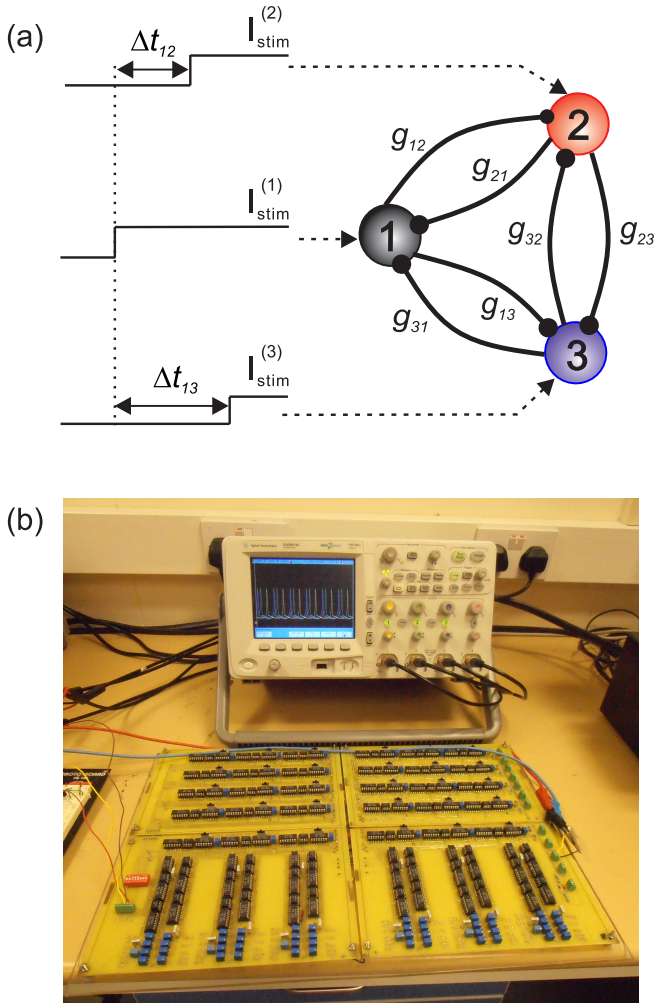

FIG. 3. (color online) (a) Timed current steps applied to neurons 1, 2 and 3. Neurons also receive postsynaptic currents from the reciprocally inhibitory links interconnecting them. (b) Circuit board.

tions synchronize [33]. The following set of conductances $g_{12} = g_{23} = g_{31} = 16\mu$S, $g_{21} = g_{13} = g_{32} = 45\mu$S was chosen which project inhibition predominantly in the anti-clockwise direction.

III. RESULTS

We next construct the phase lag maps of the CPG by recording the dephasing of neuron 2 (Φ_{21}) and neuron 3 (Φ_{31}) relative to neuron 1. Labelling the interspike intervals of neuron 1, $n = 1, 2, 3...$ from the first oscillation onwards, the state of coordinates (Φ_{21},Φ_{31}) follows a trajectory in phase space beginning from the unstable initial state prepared by timed current steps at $n = 1$, and ending in the stable final state corresponding to steady state oscillations at $n \to \infty$. A typical set of neuron oscillations is shown in Fig.4(a) for initial conditions: $\Delta t_{12} = 0.6T$, $\Delta t_{13} = 0.7T$. Transient oscillations are observed during the first 17ms ($n \leq 6$) followed by steady state oscillations. The dephasings and interspike intervals observed during the transient regime strongly depend on initial conditions. Changes in initial conditions may also cause trajectories to bifurcate towards different final states. The phase lag trajectory extracted from Fig.4(a) is shown in Fig.4(b).

Fig.4(c) shows the time dependence of the network state projected on the axes representing the three neuron voltages. The state describes loops which evolve towards a dynamic limit cycle (red line). Within the first loop $n = 1$, neurons 2 and 3 oscillate approximately in phase. A phase slip then occurs which causes a transient triphasic pattern at $n = 2, 3, 4$. This is followed by another phase slip at $n = 5, 6$ which brings neuron 1 approximately in phase with neuron 2 to produce the final stable orbit. This limit cycle corresponds to neurons firing in a clockwise sequence $1 \to 2 \to 3$ and forms one of the dynamic attractors of our CPG.

Fig.5(a) shows the phase lag map obtained by plotting the dynamic state trajectories ($\Phi_{21}(n)$,$\Phi_{31}(n)$) from every starting point. The synaptic conductances are g_{12}=g_{23}=g_{31}=16μS, g_{21}=g_{13}=g_{32}=45μS and the magnitude of the current stimulus is 100μA. The firing frequency of a neuron is 360Hz (T = 2.80ms). The phase lag map shows all trajectories to be attracted to two fixed points: attractor 3 ↻ at ($\Phi_{21} \approx 0.16$, $\Phi_{31} \approx 0.49$), and attractor 2 ↺ at (0.62, 0.30). The waveforms corresponding to these attractors are shown in Fig.5(b). Attractor 3 ↻ corresponds to a clockwise firing sequence $1 \to 2 \longrightarrow 3$ in which neuron 2 fires immediately after neuron 1 but out of phase with 3. Attractor 2 ↺ corresponds to an anticlockwise sequence $1 \to 3 \longrightarrow 2$ where neuron 3 fires immediately after 1 and out of phase with 2. We label attractors with the number of the neuron firing out of phase with the other two followed by the firing direction. The wider basin of attraction surrounding 3 ↻, implies that this attractor is the most stable of the two. The wider area of the clockwise basin is consistent with weaker clockwise projecting inhibitory links which favours clockwise pulse propagation. Phase lag maps form quadrants of dimensions $T \times T$ which repeat periodically (not shown). The first interspike intervals in the transient regime tend to have a longer period than the period of steady state oscillations T. This is why a number of state trajectories in Fig.5(a) begin in a neighboring quadrant.

We then study the effect of weakening the asymmetry of interconnects. Fig.6(a) shows the phase lag maps observed after increasing the strength of clockwise projecting inhibitory links from 16μS to g_{12}=23.5 μS, g_{23}=20 μS, g_{31}=20 μS and decreasing the strength of anticlockwise links from 45μS to g_{21}=37.2 μS, g_{13}=45 μS, g_{32}=39 μS. This network supports three attractors. The new attractor 1 ↻ is observed at coordinates (0.74, 0.34) between attractors 3 ↻ (0.21, 0.56) and 2 ↺ (0.43, 0.61). The voltage waveforms associated with 1 ↻ (Fig.6(b)) indicate a $1 \longrightarrow 2 \to 3$ sequence where neuron 3 and 2 fire

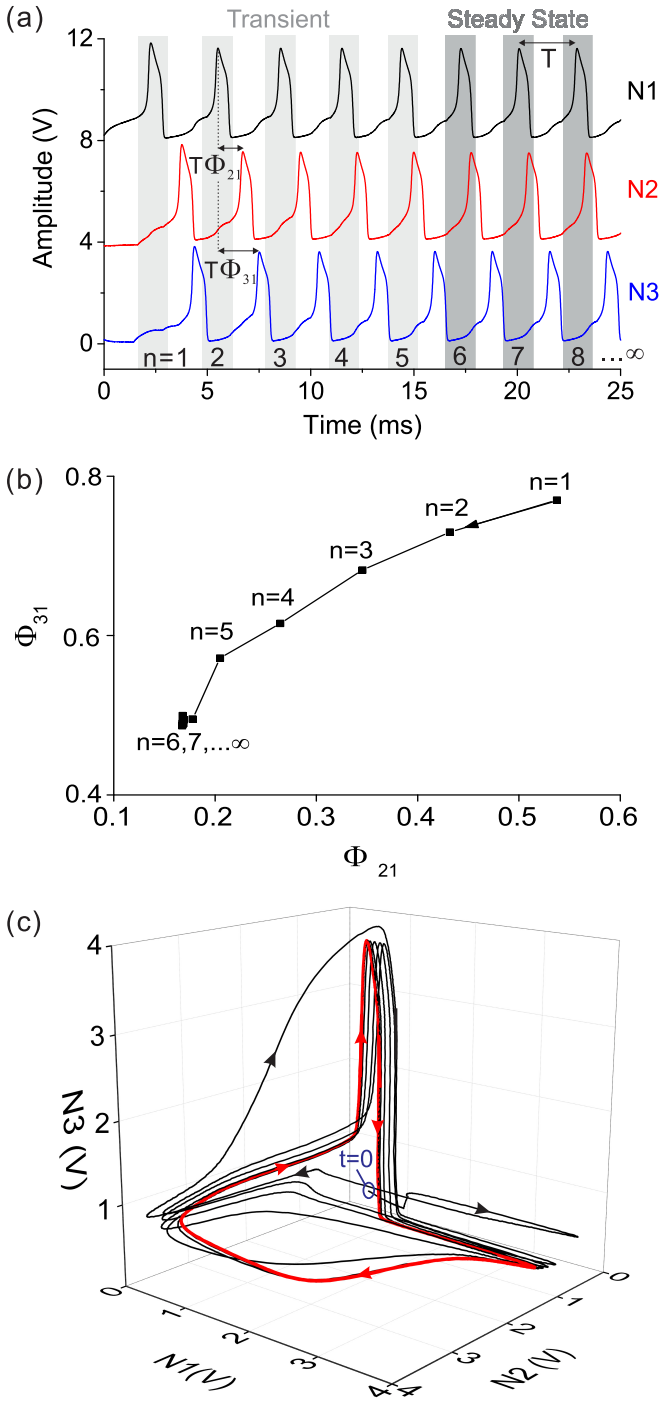

FIG. 4. (color online) (a) Transient voltage oscillations of individual neurons stimulated by 100 μA current steps delayed by $\Delta t_{12} = 0.6T$ and $\Delta t_{13} = 0.7T$. The index n counts the interspike intervals of neuron 1. (b) Phase response trajectory plotting the dephasing between neurons 3 and 1 as a function of the dephasing between neurons 2 and 1. Initial conditions are the same as in (a). (c) Trajectory of the dynamic state evolving towards a limit cycle (red closed loop). Synaptic conductance: $g_{12} = g_{23} = g_{31} = 16\mu$S, $g_{21} = g_{13} = g_{32} = 45\mu$S.

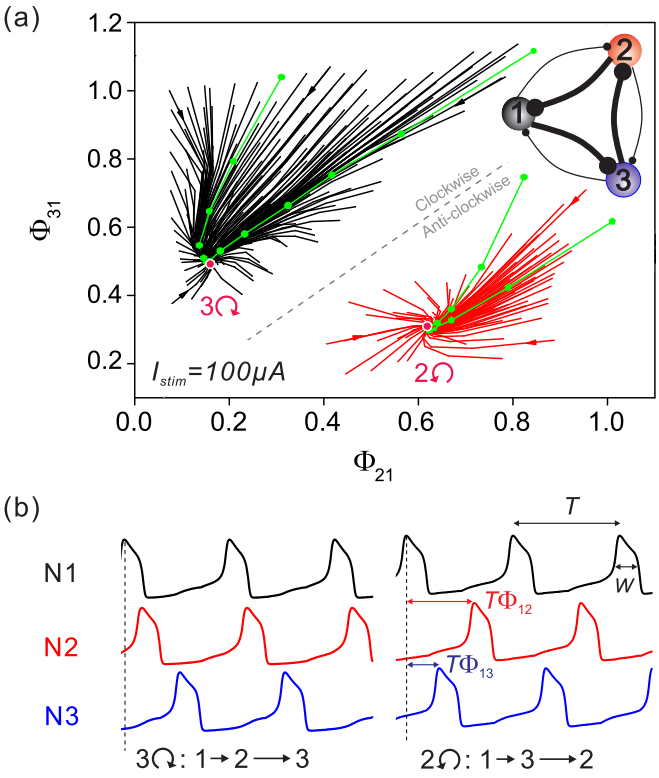

FIG. 5. (color online) (a) Phase lag map of a 3 neuron CPG with reciprocally inhibitory links projecting predominantly in the anticlockwise direction. Initial conditions for each trajectory are set by the relative timings Δt_{12} and Δt_{13} which we vary from 0 to T in steps of $0.05T$. T=2.80ms is the period of the oscillations of neuron 1 in the steady state. Two attractors are observed at 3 ↻ (0.16, 0.49) and 2 ↺ (0.62, 0.30) which correspond to clockwise and anti-clockwise firing sequences. (b) Waveforms of attractors 3 ↻ and 2 ↺. Synaptic conductances: g_{12}=g_{23}=g_{31}=16μS and g_{21}=g_{13}=g_{31}=45μS.

consecutively and out of phase with neuron 1. Within experimental error, attractors 3 ↻ and 2 ↺ have the same firing sequence and phase lags as in (Fig.5(b)).

Lowering the asymmetry of interconnects also extends the duration of transient oscillations. This is seen in the longer phase lag trajectories of Fig.6(a). The basin surrounding attractor 3 ↻ splits into two basins centered on 3 ↻ and 1 ↻ each. It therefore appears that attractor 1 ↻ is relatively unstable compared to 3 ↻ but is stabilized by making interconnects more symmetrical. Increasing the amplitude of current stimulation has the opposite effect as 1 ↻ is washed off again when I_{stim} is increased from 100μA to 120μA, the interconnect conductances remaining equal (Fig.7). Similar observation is made when I_{stim} =140μA.

When clockwise and anticlockwise projecting conductances approach a common value of g_{ij} = 30μS, all attractors vanish. Instead the CPG exhibits a single state where all neurons oscillate in phase. We interpret this result as the dynamics switching from chaotic to regular and the network collapsing into a single synchronized

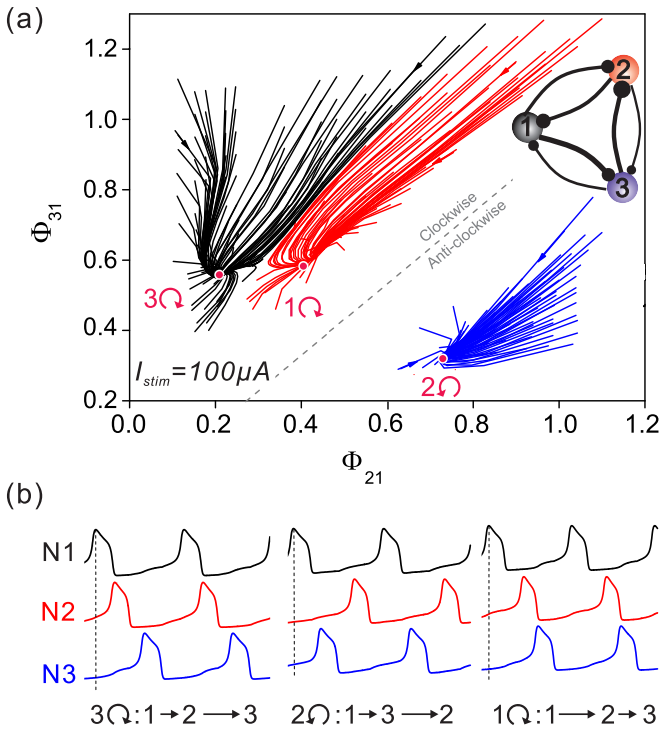

FIG. 6. (color online) (a) Phase lag map obtained by weakening the asymmetry of reciprocally inhibitory links through increases in clockwise inhibition from 16μS to g_{12} = 23μS, g_{23} = g_{31} = 20μS and decreasing anticlockwise inhibition from 45μS to g_{21} = 37μS, g_{13} = 45μS, g_{32} = 39μS. The period of neuron 1 remains T=2.80ms. Three attractors are observed at coordinates: 3 ↻ (0.21, 0.56), 1 ↻ (0.43, 0.61) and 2 ↺ (0.74, 0.34). (b) Spatio-temporal oscillations corresponding to the three attractors.

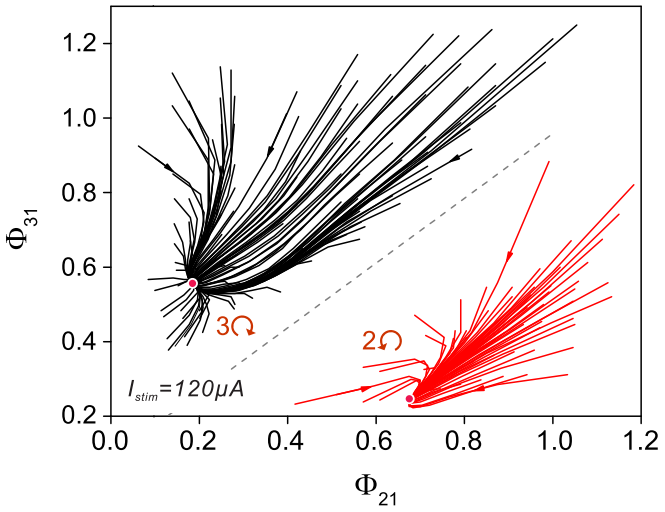

FIG. 7. (color online) Dependence of phase lag maps on the amplitude of current stimulation. The network connectivity is identical to Fig.6(a) but the current amplitude is increased from I_{stim} = 100μA to 120μA. Oscillation period: T=2.2ms.

state [33].

IV. INTERPRETATION

Our results demonstrate several features predicted by theory for a ring of 3 neuronal oscillators [16, 19]. However the experiment reveals differences concerning the nature of the oscillation patterns and their robustness to external perturbations. Wojcik et al. [19] predict 5 possible attractors including 2 triphasic rhythmic patterns (clockwise: $1 \to 2 \to 3$, anti-clockwise: $1 \to 3 \to 2$) and 3 biphasic rhythmic patterns ($1 \perp [2 \parallel 3]$, $2 \perp [3 \parallel 1]$ and $3 \perp [1 \parallel 2]$). Canavier et al [16] predict 3 attractors which comprise a synchronized state where all neurons fire in phase: (Φ_{21}, Φ_{31})=(0,0) in addition to the clockwise and anticlockwise sequences.

Our findings concur with both theories in showing that triphasic patterns are the most robust. Our experiment however shows that the 3 neurons do not fire at equally spaced intervals within the oscillation period. Instead, all waveforms in Figs.5 and 6(b) have 2 neurons firing in quick succession out-of-phase with the third. These peculiar sequences arise because our links, which mimic gap junctions, have both a dominant inhibitory character when $V_{pre} > V_{post}$ and may inject an excitatory postsynaptic current when $V_{pre} < V_{post}$. This biphasic behavior has been observed in actual gap junctions [31]. Inhibitory action obviously prevents neurons from firing at the same time hence maximizes interspike intervals by effectively acting as a repulsive force. As a neuron returns to its quiescent state, it applies transient excitatory action to the next neuron in the sequence as $V_{pre} < V_{post}$. This secondary excitatory action effectively behaves as an attractive force between spikes. The stable state that minimizes the energy of the network in the presence of these antagonist forces consists of non equidistant pulses where two neurons fire consecutively out of phase with the third. The pairing of consecutive spikes makes it necessary to consider the spike width, W, when predicting stable modes of oscillation. Defining $\zeta \equiv W/T$ as the spike width normalized by the period, there are three possible sequences corresponding to neurons 1, 2 or 3 firing out of phase with the other two (Fig.8(a)). Each sequence may carry clockwise or anticlockwise momentum depending on the order in which the two consecutive spikes appear. Including rotational degeneracy, 6 stable sequences will form with the following phase lags: 1 ↻ $(\frac{1-\zeta}{2}, \frac{1+\zeta}{2})$; 1 ↺ $(\frac{1+\zeta}{2}, \frac{1-\zeta}{2})$; 2 ↻ $(\frac{1-\zeta}{2}, 1-\zeta)$; 2 ↺ $(\frac{1+\zeta}{2}, \zeta)$; 3 ↻ $(\zeta, \frac{1+\zeta}{2})$ and 3 ↺ $(1-\zeta, \frac{1-\zeta}{2})$. From the data of Fig.5(b), we estimate $\zeta \approx 0.2$ and use this value to calculate the theoretical positions of the 6 attractors on the phase lag map. The predicted attractors are plotted in Fig.8(b) (red dots) together with the experimentally observed attractors (blue dots).

Fig.8(b) shows that the positions of the two clockwise attractors 3 ↻ and 1 ↻ are in excellent agreement with theory. Attractor 2 ↻ is apparently absent, however both

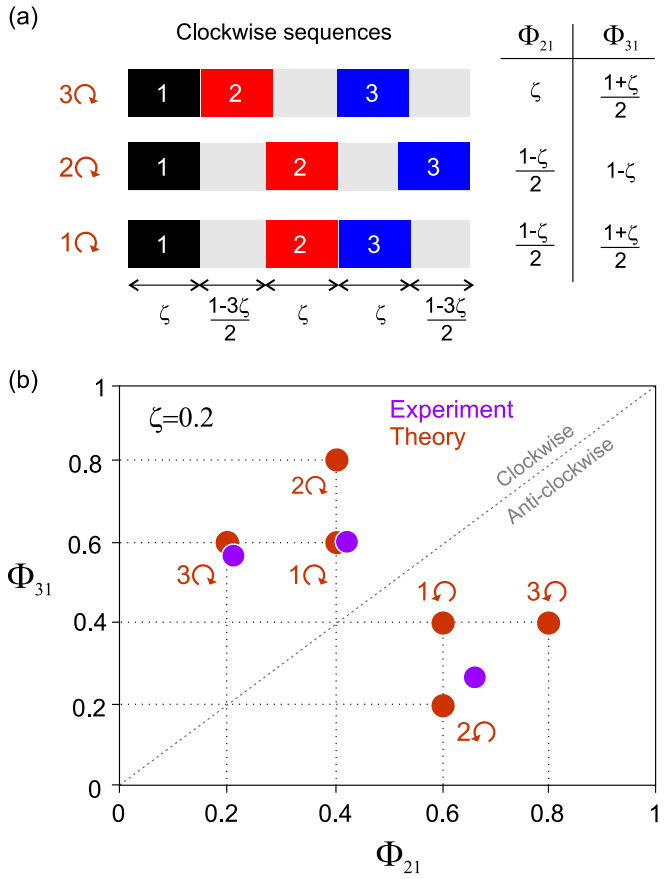

FIG. 8. (color online) (a) Rhythms in which two neurons fire in rapid succession out of phase with the third. The black, red and blue numbered blocks show the positions of spikes 1, 2 and 3 within one period of the cycle. $\zeta = W/T$ is the spike width normalized by the oscillation period. (b) Phase lag map showing the position of the theoretically predicted attractors (dots in foreground) with the experimentally observed ones (dots in background).

Figs.6 and 7 show deflected trajectories in the vicinity of (0.4,0.8) where this attractor ought to be. These deflections are likely caused by a weak local potential minimum associated with the missing attractor. The anticlockwise attractor has mainly a 2 ↺ character.

Now turning to the effects of increasing anticlockwise projecting inhibition in Figs.5 and 6, the wider clockwise basin is seen to account for a more robust clockwise firing sequence as inhibition blocks anticlockwise signal propagation. The anti-clockwise basin, however small, never vanishes in the experiment. This observation is in agreement with theory [19]. Theory also predicts that unstable attractors move from the centre to the edge of their basins of attraction when inhibition becomes stronger in one direction. This is in contrast to stable attractors which remain at the centre of their basin. This feature distinguishes the stable and unstable attractors we observe experimentally (Fig.6(a)). The unstable attractor 1 ↻ lies right at the edge of its basin of attraction whereas the stable attractor 3 ↻ is well centered. Additional motion of 1 ↻ towards the borderline caused by further increase in inhibition in one direction can explain the disappearance of this attractor from Fig.5. Not all predicted oscillation patterns could be observed, however, by equalizing clockwise and anticlockwise inhibition. This is because the network dynamics switches from chaotic to regular when reciprocal interconnects become equal. When this occurs the network dynamics collapses in a single state of collectively synchronized oscillations.

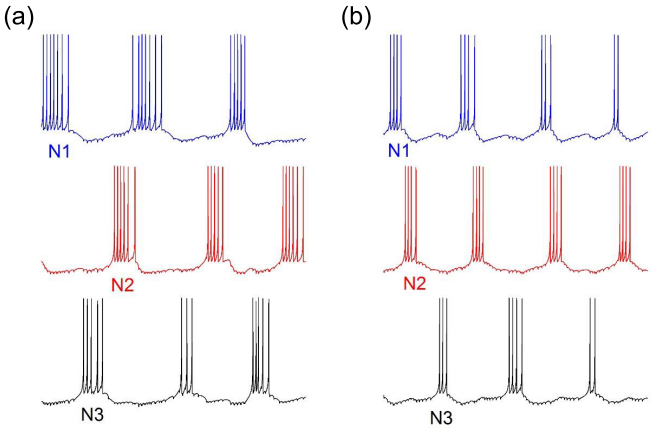

FIG. 9. (color online) (a) Anticlockwise and (b) clockwise triphasic bursting patterns produced by 3 Hindmarsh-Rose neurons coupled via mutually inhibitory links: $I_{post} = g(V_{post} - V_{pre})$ where $g > 0$.

The observation of triphasic sequences requires that the ratio of pulse width to oscillation period be $\zeta < \frac{1}{3}$. By increasing current stimulation, we increased the frequency of neuron oscillations which makes this condition harder to fulfill. We speculate, this is the reason why the unstable attractor 1 ↻ vanishes from Fig.7 when the amplitude of current stimulation increases.

The different firing sequences observed in Figs.4-7 arise from the competition between nonlinear oscillators. This competition is controlled by the network connectivity and is independent of the type of neuron used. Nonlinear oscillators other than neurons also produce multistable firing patterns as shown by Canavier et al. [16] who studied networks of Butera oscillators. To investigate the effect of substituting spiking neurons with bursting neurons, we have modelled a network of Hindmarsh-Rose neurons interconnected with the same linear couplings as in our network hardware. A simulation of a network of 3 mutually inhibitory neurons in Fig.9 shows the same stable clockwise and anticlockwise firing sequences as those of the hardware network, Figs.5(b) and 6(b). Results are therefore independent of the type of neuron used.

V. CONCLUSION

In conclusion, we have realized a ring of NaKl neurons that makes constructive use of chaos to generate stable spatio-temporal sequences activated by timed current stimuli. The multistable properties of the network are consistent with existing theories although the experiment demonstrates more subtle rhythmic patterns when mutually inhibitory links mimic gap junctions. These patterns depend on the ratio of the pulse width to the oscillation period. The results are important in that they substantiate the command neuron hypothesis [17, 18] which posits that CPG oscillations can be controlled dynamically by electrical signals [9, 21, 22]. Our experimental approach further carries significant advantages for probing the dynamics of higher dimensional networks which may be difficult to investigate numerically. Integration done according to the laws of Physics is instantaneous even in the case of larger networks implementing complex neuron models. It also bypasses limitations on the accuracy of numerical methods that rapidly creep in when multiple recovery time constants introduce stiffness in nonlinear conductance models. Real time integration of physiological feedback removes an important bottleneck to making biomedical devices for prosthetics [5] and cardiorespiratory disease [27, 28]. Much of the latter depends on properties of the triphasic respiratory oscillator in the human medulla [34, 35] whose dynamics our work helps understand.

VI. ACKNOWLEDGEMENTS

This work was supported by the British Heart Foundation under grant NH/14/1/30761.

[1] R. L. Calabrese, J. Compar. Physiol. **122**, 111 (1977).
[2] J. G. Nicholls and J. F. R. Paton, Phil. Trans. Roy. Soc. B **364**, 2447 (2009).
[3] B. E. Taylor and K. Lukowiak, Resp. Physiol. **122**, 197 (2000).
[4] A. I. Selverston, D. F. Russell, J. P. Miller, and D. G. King, Progr. Neurobiol. **7**, 215 (1976).
[5] A. Mamiya and F. Nadim, J. Neurosci. **24**, 5140 (2004).
[6] Z. Yao and O. T. Shafer, Science **343**, 1516 (2014).
[7] A. J. Ijspeert, A. Crespi, D. Ryczko, and J. M. Cabelguen, Science **315**, 1416 (2007).
[8] M. Gorassini, D. J. Bennett, O. Kiehn, T. Eken, and H. Hultborn, J. Neurophysiol. **82**, 709 (1999).
[9] A. I. Selverston, Phil. Trans. Roy. Soc. B **365**, 2329 (2010).
[10] K. Shiba, K. Nakazawa, K. Ono, and T. Umezaki, J. Neurosci. **27**, 5156 (2007).
[11] E. Marder, D. Bucher, D. J. Schulz, and A. L. Taylor, Curr. Biol. **15**, R685 (2005).
[12] M. P. Nusbaum and M. P. Beenhakker, Nature **417**, 343 (2002).
[13] M. P. Nusbaum, D. M. Blitz, A. M. Swensen, D. Wood, and E. Marder, Trends Neurosci. **24**, 146 (2001).
[14] G. B. Miles and K. T. Sillar, Physiology **26**, 393 (2011).
[15] K. Nakada, T. Asai, and Y. Amemiya, IEEE Trans. Neur. Net. **14**, 1356 (2003).
[16] C. C. Canavier, D. A. Baxter, J. W. Clark, and J. H. Byrne, Biol. Cyb. **80**, 87 (1999).
[17] C. A. G. Wiersma and K. Ikeda, Compar. Biochem. and Physiol. **12**, 509 (1964).
[18] I. Kupfermann and K. R. Weiss, Behavior Brain Sci. **1**, 3 (1978).
[19] J. Wojcik, R. Clewley, and A. Shilnikov, Phys.Rev.E **83**, 056209 (2011).
[20] J. Wojcik, J. Schwabedal, R. Clewley, and A. L. Shilnikov, PLoS ONE **9**, e92918 (2014).
[21] I. Delvolve, P. Branchereau, R. Dubuc, and J. M. Cabelguen, J. Neurophysiol. **82**, 1074 (1999).
[22] F. Delcomyn, Science **210**, 492 (1980).
[23] M. Mahowald and R. Douglas, Nature **354**, 515 (1990).
[24] G. Laurent et al., Ann. Rev. Neurosci. **24**, 263 (2001).
[25] M. Rabinovich, A. Volkovskii, P. Lecanda, H. D. I. Abarbanel, and G. Laurent, Phys.Rev.Lett. **87**, 068102 (2001).
[26] A. V. M. Herz, T. Gollisch, C. K. Machens, and D. Jaeger, Science **314**, 80 (2006).
[27] A. Nogaret, L. Zhao, D. J. A. Moraes, and J. F. R. Paton, J. Neurosci. Meth. **212**, 124 (2013).
[28] A. Nogaret et al., J. Physiol. **593**, 068102 (2015).
[29] A. L. Hodgkin and A. F. Huxley, J. Physiol. **117**, 500 (1952).
[30] M. Dhamala, V. K. Jirsa, and M. Ding, Phys.Rev.Lett. **92**, 028101 (2004).
[31] M. Galarreta and S. Hestrin, Science **292**, 2295 (2001).
[32] R. C. Elson et al., Phys.Rev.Lett. **81**, 5692 (1998).
[33] M. I. Rabinovich, P. Varona, A. I. Selverston, and H. D. I. Abarbanel, Rev. Mod. Phys. **78**, 1213 (2006).
[34] J. C. Smith, A. P. L. Abdala, H. Koizumi, I. A. Rybak, and J. F. R. Paton, J. Neurophysiol. **98**, 3370 (2007).
[35] J. C. Smith, I. A. Rybak, A. Borgmann, A. P. Abdala, and J. F. R. Paton, Trends Neurosci. **36**, 152 (2013).